Open access • Journal Article • DOI:10.1016/J.JQSRT.2018.04.026

The rank correlated FSK model for prediction of gas radiation in non-uniform media, and its relationship to the rank correlated SLW model — Source link

Vladimir P. Solovjov, Brent W. Webb, Frédéric André

Institutions: Brigham Young University, Institut national des sciences Appliquées de Lyon

Published on: 01 Jul 2018 - Journal of Quantitative Spectroscopy & Radiative Transfer (Pergamon)

Topics: Rank (linear algebra) and Frequency-shift keying

The rank correlated FSK model for prediction of gas radiation in non-uniform media

Frédéric Andre, Vladimir Solovjov, Brent Webb

The Rank Correlated FSK Model for Prediction of Gas Radiation in Non-Uniform Media

Vladimir P. Solovjov[1], Brent W. Webb[1], Frederic Andre[2]

[1]Brigham Young University, CTB-435, Provo, UT 84602 USA

[2]Centre de Thermique et d'Energétique de Lyon, INSA de Lyon – 9 rue de la Physique – 69621 Villeurbanne, France

ABSTRACT Following previous theoretical development based on the assumption of a rank correlated spectrum, the Rank Correlated Full Spectrum *k*-distribution (RC-FSK) method is proposed. The method proves advantageous in modeling radiation transfer in high temperature gases in non-uniform media in two important ways. First, and perhaps most importantly, the method requires no specification of a reference gas thermodynamic state. Second, the spectral construction of the RC-FSK model is simpler, requiring only two cumulative *k*-distributions. Further, although not exhaustive, example problems presented here suggest that the method may also yield improved accuracy relative to prior methods, and may exhibit less sensitivity to the blackbody source temperature used in the model predictions. This paper outlines the theoretical development of the RC-FSK method, comparing the spectral construction with prior correlated spectrum FSK method formulations. The work presents predictions using the new Rank Correlated FSK method and previous FSK methods in three different example problems. Line-by-line benchmark predictions are used to assess the accuracy.

Keywords

Gas radiation, rank correlation of gas absorption spectra, comonotonicity, SLW, Generalized SLW Method, Rank Correlated SLW model, Rank Correlated FSK model, FSCK, improved FSCK

1. INTRODUCTION

Global methods in modelling of radiation transfer in high temperature gases in non-isothermal, non-homogeneous media have proven to be the most computationally efficient methods for such predictions. These methods include the SLW (Spectral Line Weighted-sum-of-gray-gases) [1-3], ADF (Absorption Distribution Function) [4], FSK (Full Spectrum *k*-distribution) [5-6], and SLMB (Spectral Line Moment-Based) [7] methods. These methods can provide high accuracy of prediction of radiation transfer, often comparable to that of rigorous benchmark line-by-line (LBL) predictions but at significantly lower computational cost. Despite the seeming difference between SLW, ADF, and FSK methods, they all are based on the same fundamental principle in modelling of the gas absorption spectrum, and it has previously been shown that all can be described as particular cases of the Generalized SLW Model [8]. Despite this commonality among the methods, they still exist mainly separately having their own developments, refinements, and implementation [see, *e.g.*, 9]. Further, the literature demonstrates that all of the various global methods have been adopted for prediction of radiation transfer in engineering applications.

Recently, a significant advance in the Spectral Line Weighted-sum-of-gray-gases (SLW) method was presented for prediction of gas radiation in non-uniform gaseous media [10]. Whereas previous global methods (both FSCK and SLW) have been based on the assumption of a correlated gas absorption spectrum for the treatment of non-uniform gas media, this recently developed model proposed a modified assumption based on *rank correlation* of the absorption spectrum. Unlike all previous methods based on correlated spectra, the RC-SLW method does not require the specification of a reference gas thermodynamic state (and corresponding reference spectrum) for its implementation. Additionally, the RC-SLW method has been shown to yield greater simplicity in its construction, and appears to offer somewhat greater predictive accuracy. This paper seeks to extend the rank correlated spectrum assumption to the Full Spectrum *k*-distribution method, reformulating the approach under the rank correlated spectrum assumption within the FSK model framework.

Similar to the original SLW Reference Approach for treating gas radiation in non-uniform media, all existing versions of the FSK correlated models begin with specification of the gas

reference thermodynamic state in the domain, and this reference state is used in the construction of the spectral model. Simplistically speaking, other states in the domain are "corrected" from the reference state by invoking the correlated spectrum assumption. The method can be sensitive to the choice of reference state (principally to the gas reference temperature). There are several different approaches to define the optimal reference state, but no consistent and theoretically-based recommendation for the reference state has emerged. The proposed Rank Correlated FSK approach does not require the reference state at all for its construction. As was shown previously [11], the rank correlated approach to treating spatial variations in gas temperature is a particular case of general comonotonic methods for treating non-uniform media in high temperature gases. It is also shown that the rank correlated assumption is theoretically the optimal correlated model in such situations.

Finally, the development presented here of the FSK method using the rank correlated spectrum assumption will bring into alignment the new FSK formulation and the previously published Rank Correlated SLW model. The paper will reveal that the RC-FSK model and the RC-SLW models are identical in their theoretical foundation. This further underlines the similarities between the Full Spectrum *k*-distribution and the Spectral Line Weighted-sum-of-gray-gases models.

2. THE RANK CORRELATED SPECTRUM

2.1 Spectral Radiative Transfer Equation

Propagation of radiation in absorbing and emitting gaseous media is governed by the Radiative Transfer Equation (RTE) [1], which describes the change in spectral radiation intensity $I_\eta\left(s,\mathbf{\Omega}\right)$ along a pathlength s in a direction $\mathbf{\Omega}$:

$$\frac{\partial I_\eta\left(s,\mathbf{\Omega}\right)}{\partial s}=-\kappa_\eta\left(s\right)I_\eta\left(s,\mathbf{\Omega}\right)+\kappa_\eta\left(s\right)I_{b\eta}\left[T\left(s\right)\right] \tag{1}$$

Here, η [cm^{-1}] is the wavenumber, $I_{b\eta}\left[T\left(s\right)\right]$ is the spectral Planck blackbody intensity at the local gas temperature $T\left(s\right)$, K. The local spectral absorption coefficient is defined as $\kappa_\eta\left(s\right)=N\left(s\right)Y\left(s\right)C_\eta\left(\phi\left(s\right)\right)$, m^{-1}, where $C_\eta\left(\phi\left(s\right)\right)$, m^2/mol, is the gas absorption cross-section, and $\phi\left(s\right)=\left\{T\left(s\right),Y\left(s\right),p\left(s\right)\right\}$ is a symbolic vector notation for the definition of the local gas

thermodynamic state at temperature $T(s)$, total pressure $p(s)$, and mole fraction $Y(s)$. High resolution spectral databases such as HITEMP-2010 [12] are used to generate the spectral gas absorption cross-section $C_\eta(\phi)$.

Among the rigorous approaches for solution of the spectral RTE, Eq. (1), the simplest formulation is a line-by-line integration of the equation, subject to the detailed local gas absorption spectrum. The Line-by-Line (LBL) method solves the spectral form of the RTE for each wavenumber η, following which the total intensity of radiation is obtained by spectral integration over all wavenumbers. By contrast, global methods for modeling gas radiation begin with spectral integration of the RTE, and then solve the spectrally integrated intensity $I(s,\mathbf{\Omega})$ for a finite number of discrete values of the absorption cross-section (or absorption coefficient) as a continuous variable. To determine total radiative quantities, it may be said that global methods integrate over absorption cross-section (or absorption coefficient) rather than an integration over wavenumber.

One characterization of gas absorption spectrum $\kappa_\eta(\phi_g)$ at a given gas thermodynamic state $\phi_g = \{T, Y, p\}$ is performed with the help of the full-spectrum cumulative *k*-distribution, which can be formally defined as the Planck blackbody emissive power-weighted distribution at the blackbody source temperature T_P

$$g_{\phi,T_P}(k) = g(k,\phi,T_P) = \frac{1}{E_b(T_P)}\int_0^\infty H\left[k-\kappa_\eta(\phi)\right] E_{b\eta}(T_P)\,d\eta \tag{2}$$

where, H is the Heaviside unit-step function. The distribution function g is a strictly increasing function varying between 0 and 1 with respect to the variable k, and therefore, it is invertible. The inverse of the function $g(k,\phi,T_P)$ is the reordered absorption coefficient denoted as $k(g,\phi,T_P)$. Cumulative *k*-distribution databases have been developed for gas species of engineering interest over a wide range of thermodynamic states, and are available for use [13,14]. The distribution function g is directly related to the Absorption Line Blackbody Distribution Function (ALBDF) $F(C,\phi_g,T_b=T_P)$ used as basis in the SLW method. The ALBDF is a function of absorption cross-section C, and g used in the FSK method can be obtained from F by a simple change of variable $C = R_u T_g k/pY$, where R_u is the universal gas constant [1]. Like the ALBDF, the distribution function $g(k,\phi,T_P)$ is calculated in advance from the high-resolution

gas absorption cross-section, and has recently been presented in tabulated form or mathematical correlations [15] generated using one of the most up-to-date high temperature spectral database, HITEMP 2010 [12].

2.2 Correlated Gas Absorption Coefficients

Global methods in gas radiation deal with spectral integration of the monochromatic RTE over all wavenumbers, which can be performed without appearance of additional Leibnitz terms of integration if some ideal dependence of gas absorption spectra is assumed. Until recently, the assumption of a correlated absorption spectrum [3,16] was used in the solution of the spectral RTE by formulating the dependence of the gas absorption coefficient (or absorption cross-section) at the local thermodynamic state ϕ_{loc} (or simply ϕ) on the absorption coefficient at some chosen reference thermodynamic state $\phi_{ref} = \phi_0$ through solution of an implicit equation. The FSK method expresses this correlated dependence by the equation in terms of the *g*-distribution

$$g\left(k,\phi,T_0\right) = g\left(k_0,\phi_0,T_0\right) \tag{3}$$

while the SLW method presents an equivalent relationship in terms of the ALBDF (expressed in the nomenclature commonly used with the SLW method)

$$F\left(C_{loc},\phi_{loc},T_b\right) = F\left(C_{ref},\phi_{ref},T_b\right) \tag{4}$$

These implicit equations are necessarily established at the same, fixed blackbody source temperature, T_0 for Eq. (3) and T_b for Eq. (4), providing that the fraction of the total emissive power $E_{b\eta}\left(T_b\right)$, which corresponds to the intervals of wavenumbers where $\kappa_\eta\left(\phi\right) < k$ remains the same at any local state ϕ. Under this assumption, the spectral absorption coefficient is loosely said to be correlated.

Further development of the FSK model in non-uniform media can be achieved by modification of the assumption of correlated spectrum discussed in [3,16] to a less restrictive assumption of rank correlation of the absorption spectra at different thermodynamic states. The *rank correlated spectrum* assumption is defined as follows: Let ϕ_1 and ϕ_2 represent two arbitrary gas thermodynamic states, and let $\Delta_1 = \left\{\eta : \kappa_\eta\left(\phi_1\right) < \kappa_{\eta'}\left(\phi_1\right)\right\}$ and $\Delta_2 = \left\{\eta : \kappa_\eta\left(\phi_2\right) < \kappa_{\eta'}\left(\phi_2\right)\right\}$ be the wavenumber intervals defined by the values of absorption coefficients $\kappa_{\eta'}\left(\phi_1\right)$ and $\kappa_{\eta'}\left(\phi_2\right)$ at the

same arbitrary value of wavenumber η'. If the intervals are identical, $\Delta_1 = \Delta_2$, the spectra $\kappa_\eta(\phi_1)$ and $\kappa_\eta(\phi_2)$ are said to be rank correlated. Neither of the thermodynamic states ϕ_1 and ϕ_2 is designated as a reference state. Rank correlation establishes the relationship between the gas absorption coefficients at two arbitrary local gas thermodynamic states, and in contrast to a definition of correlated spectra, it does not require specification of any reference thermodynamic state and corresponding reference absorption spectrum.

The implication of the rank correlated spectrum on the cumulative *k*-distribution (whose inverse is also referred to as the reordered absorption coefficient) may be described as follows. Consider in Fig. 1 the reordered absorption coefficient at different thermodynamic states ϕ_1 and ϕ_2 for the same fixed blackbody source temperature T_P, given as $k(g,\phi_1,T_P)$ and $k(g,\phi_2,T_P)$. According to the assumption of a rank correlated spectrum, for a fixed value of the *g*-variable and fixed blackbody source temperature T_P, the wavenumber intervals are defined as follows

$$\left\{\eta:\ \kappa_\eta(\phi_1) < k(g,\phi_1,T_P)\right\} = \left\{\eta:\ \kappa_\eta(\phi_2) < k(g,\phi_2,T_P)\right\} = \Delta \tag{5}$$

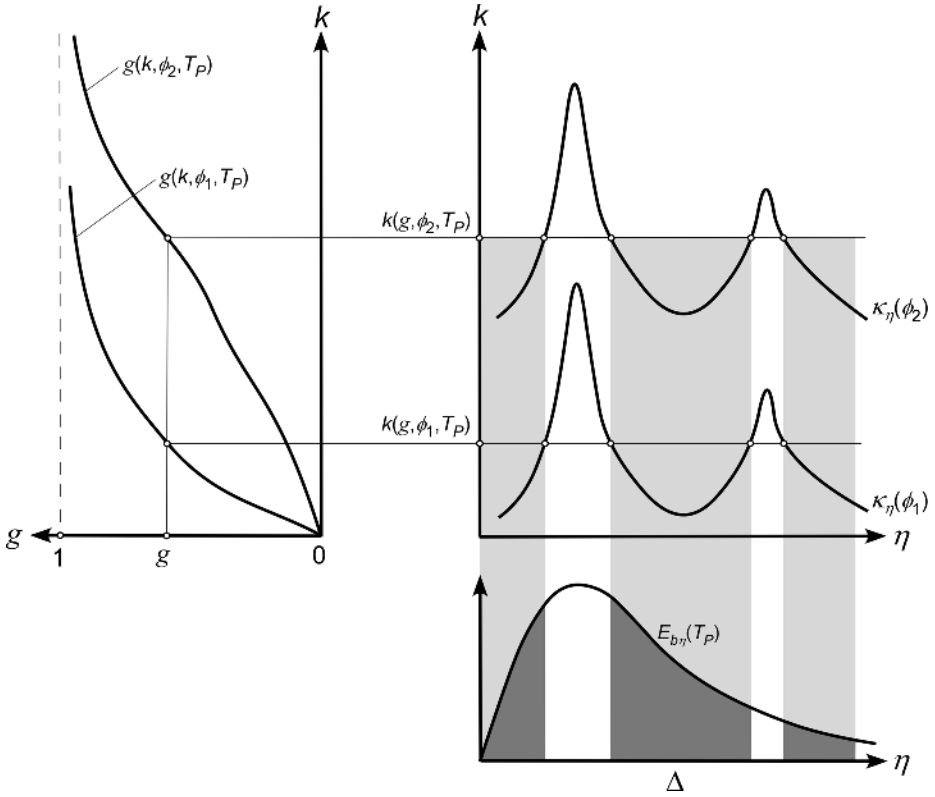

Figure 1. Rank correlated reordered absorption coefficients.

The wavenumber intervals defined by the relation given in Eq. (5) for the spectra at the two arbitrary thermodynamic states are thus identical. Because of this property, the set of discrete reordered absorption coefficients $k\left(g,\phi_m,T_P\right)$, $m=1,2,...$ can be defined as the rank correlated or *co-monotonic reordered continuous absorption coefficients* as depicted in Fig. 1. The thermodynamic states ϕ_m can be any local thermodynamic state in the medium.

The concept of rank correlated reordered absorption coefficient $k\left(g,\phi_m,T_P\right)$ considered in this work is a particular case of a more general approach to *co-monotonic global spectral modelling* of gas radiation in non-uniform media based on arbitrary probability measures [11], where it can be shown that if two arbitrary constants $k_1,k_2>0$, one of two conditions exists

$$\left\{\eta:\kappa_\eta\left(\phi_1\right)<k_1\right\}\subseteq\left\{\eta:\kappa_\eta\left(\phi_2\right)<k_2\right\} \quad \text{or} \quad \left\{\eta:\kappa_\eta\left(\phi_1\right)<k_1\right\}\supseteq\left\{\eta:\kappa_\eta\left(\phi_2\right)<k_2\right\} \tag{6}$$

and the corresponding spectral absorption coefficients $\kappa_\eta\left(\phi_1\right)$ and $\kappa_\eta\left(\phi_2\right)$ are co-monotonic (for common monotonicity). More detail on the theoretical construct of rank correlation and comonotonicity of absorption spectrum can be found in refs. [10,11].

2.3 Current Correlated FSK Models

A brief review of the construction of the correlated FSK models as detailed in [5-6, 17-18] is first presented here. The spectral RTE, Eq. (1), reordered with respect to the *k*-distribution function, becomes the correlated RTE of the FSK method (where the intensity's dependence on *s* and **Ω** are omitted for brevity):

$$\frac{\partial I_{g_0}}{\partial s}=-k^*\left(g_0\right)I_{g_0}+k^*\left(g_0\right)a\left(g_0\right)I_b\left(T\right) \tag{7}$$

where

g_0 is the current value of the spectral *g*-variable

I_{g_0} is the intensity as a function of continuous *g*-variable

$I_b\left(T\right)=\sigma T^4/\pi$ is the total Planck blackbody intensity

$k^*\left(g_0\right)$ is the local absorption coefficient

$a\left(g_0\right)$ is the local stretching factor (weighting function)

According to the development in ref. [16], the Full Spectrum Correlated *k*-distribution (FSCK) model consists of the following: For a given current value of the continuous *g*-variable g_0, one must find the corresponding local values of the absorption coefficient $k^*\left(g_0\right)$ and the local value of the *k*-distribution *g* which will define the local stretching factor $a\left(g_0\right)$ needed in the solution of Eq. (7). Currently, there exist two versions of the FSCK model which will now be summarized briefly.

FSCK-I Model. The first Full Spectrum Correlated *k*-distribution model was introduced by Zhang and Modest [5,6], and will be denoted here the FSCK-I model. As shown in Fig. 2a, construction of the FSCK-I model consists of three steps **A** – **B** – **C**:

A for a given value of g_0, calculate k_0 by solving the equation $g\left(k_0,\phi_0,T_0\right)=g_0$

B calculate the local value of k_{I}^* by solving the equation $g\left(k_{\mathrm{I}}^*,\phi,T_0\right)=g\left(k_0,\phi_0,T_0\right)$

C calculate the local value of *g* from $g=g\left(k_0,\phi_0,T\right)$

The evaluation of three different *k*-distribution functions is required for the construction of the FSCK-I model. The assumption of spectral correlation at step **A** – **B**, expressed by the implicit relation $g\left(k_{\mathrm{I}}^*,\phi,T_0\right)=g\left(k_0,\phi_0,T_0\right)$, is established at the reference blackbody source temperature $T_P=T_0$. Note that this model can be equivalently modified to a sequence of steps **B** – **A** – **C** shown schematically in Fig. 2a, retaining the same calculations and result.

FSCK-II Model. A refined and improved correlated FSK model was introduced in the paper of Cai and Modest [18], and was termed the Improved FSCK model (denoted here the FSCK-II model). As shown in [18] and illustrated schematically in Fig. 2b, construction of the FSCK-II model consists of steps **A** – **A′** – **B′** – **A′**, and summarized in the following steps:

A for a given value of g_0, calculate k_0 by solving the equation $g\left(k_0,\phi_0,T_0\right)=g_0$

A′ calculate the local value of *g* as $g=g\left(k_0,\phi_0,T\right)$

B′ calculate the local value of k_{II}^* by solving the equation $g\left(k_{\mathrm{II}}^*,\phi,T\right)=g\left(k_0,\phi_0,T\right)$

A′ calculate the local value of *g* as $g=g\left(k_{\mathrm{II}}^*,\phi,T\right)$

Three *k*-distribution functions are involved, and the assumption of correlation of the spectrum is invoked in step **A′** – **B′** by the relation $g\left(k_{\text{II}}^{*},\phi,T\right)=g\left(k_0,\phi_0,T\right)$. This equality is established at the local blackbody source temperature $T = T_P$. The last step of the FSCK-I model construction appears to be redundant because it returns the same value of g which was already calculated at point **A′** at the reference gas thermodynamic state. It may be mentioned that the FSCK-II model has been shown to be equivalent to Method II.2.2 in ref. [10]. The work of Cai and Modest demonstrated that the FSCK-II model yields considerable improvements in accuracy over the FSCK-I model [18].

Figure 2 illustrates that for construction of each FSCK model, three *k*-distribution functions are needed, namely,

FSCK-I model: $g\left(k,\phi_0,T_0\right)$, $g\left(k,\phi_0,T\right)$, and $g\left(k,\phi,T_0\right)$

FSCK-II model: $g\left(k,\phi_0,T_0\right)$, $g\left(k,\phi_0,T\right)$, and $g\left(k,\phi,T\right)$

Two of the distribution functions are common for both approaches. It should be underlined that the gas reference state ϕ_0 must be specified for the construction of both the FSCK-I model and the FSCK-II model.

2.4 The Rank Correlated FSK (RC-FSK) Model

The Rank Correlated FSK model presented here is a direct reformulation of the continuous limit of the Rank Correlated SLW model in terms of the full-spectrum *k*-distribution model framework. The theoretical foundation and detailed derivation of the Rank Correlated SLW method are given in [8,10-11].

As shown in Fig. 3, the Rank Correlated FSK (RC-FSK) spectral model is constructed in two simple steps denoted **B** – **B′**:

B for a given value g_0, calculate the local absorption coefficient $\kappa^{*}=k\left(g_0,\phi,T_P\right)$

B′ calculate the local value of the *g*-distribution $g=g\left(\kappa^{*},\phi,T\right)$

This calculation sequence as illustrated in Fig. 3 shows that only two cumulative distribution functions are needed for construction of the Rank Correlated FSK model. No reference thermodynamic state or reference spectrum is involved in its implementation.

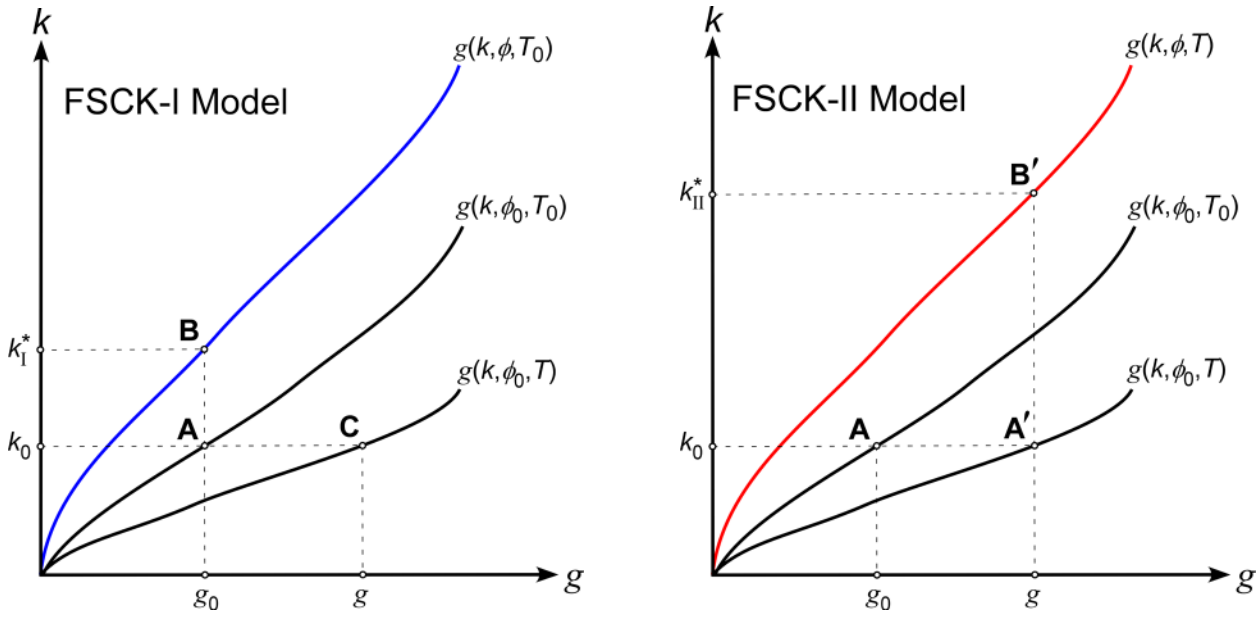

Figure 2. Construction of a) the FSCK-I spectral model (correlated step is **A** – **B**), and b) the FSCK-II spectral model (correlated step is **A′** – **B′**).

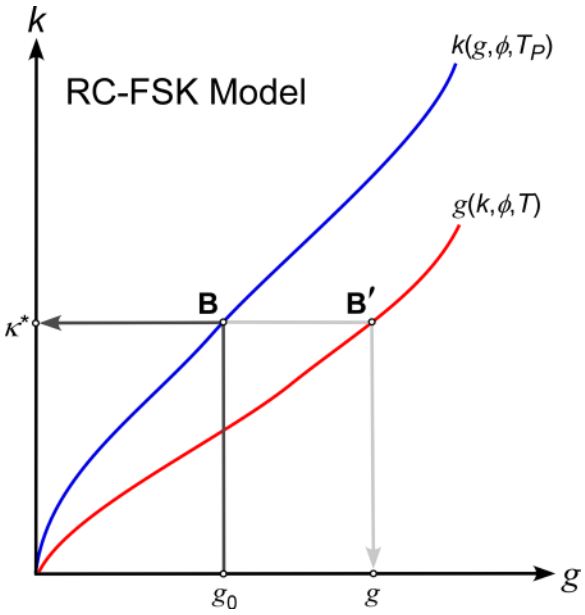

Figure 3. The Rank Correlated FSK spectral model. The current value of the variable g_0 provides rank correlation of *k*-distributions at all gas local states (correlated step is **B** – **B′**).

Once the RTE has been solved the total intensity can be found by integration over g_0:

$$I = \int_0^1 I_{g_0}\, dg_0 \tag{8}$$

In the Rank Correlated FSK model, the stretching factor $a\left(g_0\right)$ appearing in the RTE, Eq. (7), is defined as

$$a\left(g_0\right) = \frac{\partial}{\partial g_0} g\left[k\left(g_0,\phi,T_P\right),\phi,T\right] \tag{9}$$

For numerical solution, the expression for $a\left(g_0\right)$ given by Eq. (9) can be discretized, yielding

$$\frac{\partial I_j}{\partial s} = -\kappa_j^* I_j + \kappa_j^* \frac{g\left[k\left(g_j,\phi,T_P\right),\phi,T\right] - g\left[k\left(g_{j-1},\phi,T_P\right),\phi,T\right]}{\Delta g} I_b\left(T\right) \tag{10}$$

where g_j are the discrete partition values of g in the interval [0,1], and $\Delta g = g_j - g_{j-1}$. This finite difference representation of the weighing factor was shown previously in section 4.5 of ref. [8]. Once Eq. (10) is solved the total intensity of radiation is then found as

$$I = \int_0^1 I_{g_0} dg_0 = \sum_j I_j\, \Delta g \tag{11}$$

Upon integration over the spectrum (integration over g_0) the emission term of the reordered RTE, Eq. (7), becomes

$$\int \kappa^*\left(g_0\right) \frac{\partial g\left(\kappa^*,\phi,T\right)}{\partial g_0} I_b\left(T\right)\, dg_0 \approx I_b\left(T\right) \sum_j \kappa_j^* \Delta g = I_b\left(T\right) \kappa_P\left(\phi,T\right) \tag{12}$$

where $\kappa_P\left(\phi,T\right)$ is a modified Planck mean absorption coefficient evaluated at the local gas thermodynamic state, and the blackbody source temperature is the local gas temperature, $T = T_P$. The integration of this term shows that the Rank Correlated FSK approach rigorously preserves the local emission term when the RTE is integrated over the spectrum.

2.5 Relationship between the RC-FSK and the RC-SLW Models

As previously mentioned, the Rank Correlated FSK model presented here is a direct reformulation of the continuous limit of the Rank Correlated SLW model in terms of full-spectrum *k*-distributions. However, in practice the classical SLW model begins with discretization of the continuous absorption cross-section spectrum into gray gases. Therefore, the discrete

version of the Rank Correlated FSK model, Eq. (10), can now be related to the corresponding Rank Correlated SLW model. One can multiply the RC-FSK RTE, Eq. (10), by the finite increment Δg. If in the resulting equation one then denotes $I_j^{loc} = I_j \Delta g$ as the SLW gray gas intensity, $\kappa_j^{loc} = \kappa_j^*$ as the gray gas absorption coefficient, and the finite difference $a_j^{loc} = g\left[k\left(g_j, \phi, T_P\right), \phi, T\right] - g\left[k\left(g_{j-1}, \phi, T_P\right), \phi, T\right]$ as the local gray gas weights, the equation becomes the Rank Correlated SLW RTE [10]:

$$\frac{\partial I_j^{loc}}{\partial s} = -\kappa_j^{loc} I_j^{loc} + \kappa_j^{loc} a_j^{loc} I_b^{loc} \tag{13}$$

Similar to the RC-FSK method outlined in the foregoing sections, the Rank Correlated SLW spectral model consists of two simple steps as illustrated in Fig. 4.

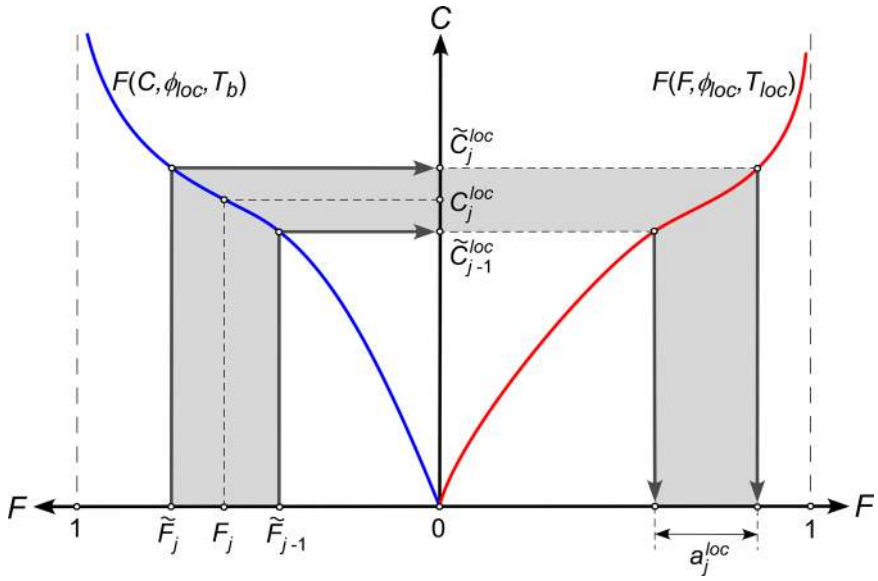

Figure 4. Graphical illustration of construction of the Rank Correlated SLW spectral model.

In this calculation sequence only two distribution functions are needed:

1) For partition of the F-variable into fixed values $\tilde{F}_j$ for $j = 0,1,2,\ldots,n$ and F_j for $j = 1,2,\ldots,n$, one calculates the local supplemental absorption cross-sections using the inverse Absorption Line Blackbody Distribution Function (ALBDF):

$$C_j^{loc} = C\left(F_j, \phi_{loc}, T_b\right) \tag{14a}$$

$$\tilde{C}_j^{loc} = C\left(\tilde{F}_j, \phi_{loc}, T_b\right) \tag{14b}$$

2) Calculate the local gray gas weights with the help of the ALBDF

$$a_j^{loc} = F\left(\tilde{C}_j^{loc}, \phi_{loc}, T_{loc}\right) - F\left(\tilde{C}_{j-1}^{loc}, \phi_{loc}, T_{loc}\right) \tag{15}$$

The gray gas absorption coefficients in Eq. (15) are $\kappa_j^{loc} = N^{loc} Y^{loc} C_j^{loc}$, where N^{loc} is the local gas molar density. As demonstrated previously in the development of the RC-SLW model [10], no specification of the gas reference state is required. It was shown in [10] that with an increase in the number of gray gases, the Rank Correlated SLW model approaches its continuous limit.

This finding is important as it demonstrates that the rank correlated formulation of the FSK model and the RC-SLW model are identical, and when implemented using the same discretization of the appropriate variables *g* or *F*, respectively (and when using the same cumulative distribution functions database), the two models will produce identical predictions.

3. MODEL VALIDATION

This section illustrates the use of the FSCK-I, FSCK-II, and RC-FSK (equivalent to RC-SLW) models presented in the foregoing sections in three example problems designed to test their accuracy over a range of problem parameters and compare the models' performance. The basis for assessing accuracy in all three example problems is the line-by-line (LBL) prediction of radiative transfer. The benchmark line-by-line predictions were obtained using the spectral information generated from the HITEMP-2010 spectroscopic database [12]. The absorption coefficient was compiled at discrete wavenumber values with a spectral step $\Delta\eta$ = 0.01 cm^{-1}. More details on the line-by-line modelling can be found in [19,20].

The cumulative *k*-distributions used for the FSK modelling carried out here were calculated using the ALBDF lookup table described in [15]. Thus, the same spectral database was used for generation of the *k*-distribution functions (its SLW counterpart, the ALBDF) and the line-by-line solutions of the RTE. Numerical spectral integration in the FSK modeling for all formulations was performed using discretization of the *g*-variable interval [0,1] into 25 Gauss-Legendre quadrature nodes, and solution of the discretized RTE Eq. (10) is carried out using the analytical multilayer approach [19] for all three example problems.

Examples 1 and 2 in the results section to follow consider one-dimensional radiative transfer in a plane parallel layer of thickness L = 1.0 m bounded by black walls and filled with pure water vapor. For these two example problems gas mixtures were deliberately avoided so as to eliminate any additional error arising from further assumptions needed to treat multiple gases in the system (error beyond those arising solely from a correlated spectrum assumption). Example 3 explores radiative transfer in a two-layer system with a uniform mixture of H_2O and CO_2 but with radically different temperatures in each layer.

In the correlated FSK model predictions where the spatial average temperature is used as the reference temperature T_0 the average temperature was determined from its definition

$$T_{ave} = \frac{1}{L}\int_0^L T(x)\,dx \tag{16}$$

Example 1. Single wave profile of temperature and gas composition

The first example problem studies prediction of the local divergence of total net radiative flux in a plane-parallel layer of thickness L = 1.0 m bounded by black walls and filled with water vapor at total pressure p = 1.0 atm. Simulations have been carried out for the total net radiative wall flux and the local divergence of the total net radiative flux in the layer. Single wave sinusoidal gas temperature and water vapor fraction profiles are imposed in the layer:

$$T(x) = \frac{T_{\max}+T_{\min}}{2} + \frac{T_{\max}-T_{\min}}{2}\cos\left[\frac{2\pi}{L}\left(x-\frac{L}{2}\right)\right], \text{ K} \tag{17a}$$

$$Y(x) = \frac{Y_{\max}+Y_{\min}}{2} + \frac{Y_{\max}-Y_{\min}}{2}\cos\left[\frac{2\pi}{L}\left(x-\frac{L}{2}\right)\right] \tag{17b}$$

Wall temperatures are given as $T(0) = T(L) = T_{\min}$, K. This single wave profile considered here, as well as the double wave profile in the next example, has the property that the spatial average temperature and spatial average mole fraction are easily determined from the relations

$$T_{ave} = \left(T_{\max}+T_{\min}\right)/2 \quad \text{and} \quad Y_{ave} = \left(Y_{\max}+Y_{\min}\right)/2 \tag{18}$$

As shown graphically in Fig. 5, two cases are considered for Example 1 using the temperature and H_2O mole fraction profiles of Eqs. (17a) and (17b) but with different $T_{\max}$ and $Y_{\max}$:

Case 1a: $T_{\min} = 300$ K, $T_{\max} = 1300$ K ($T_{ave} = 800$ K), $Y_{\min} = 0.1$, $Y_{\max} = 0.2$ ($Y_{ave} = 0.15$)

Case 1b: $T_{\min} = 300$ K, $T_{\max} = 2300$ K ($T_{ave} = 1300$ K), $Y_{\min} = 0.1$, $Y_{\max} = 0.4$ ($Y_{ave} = 0.25$)

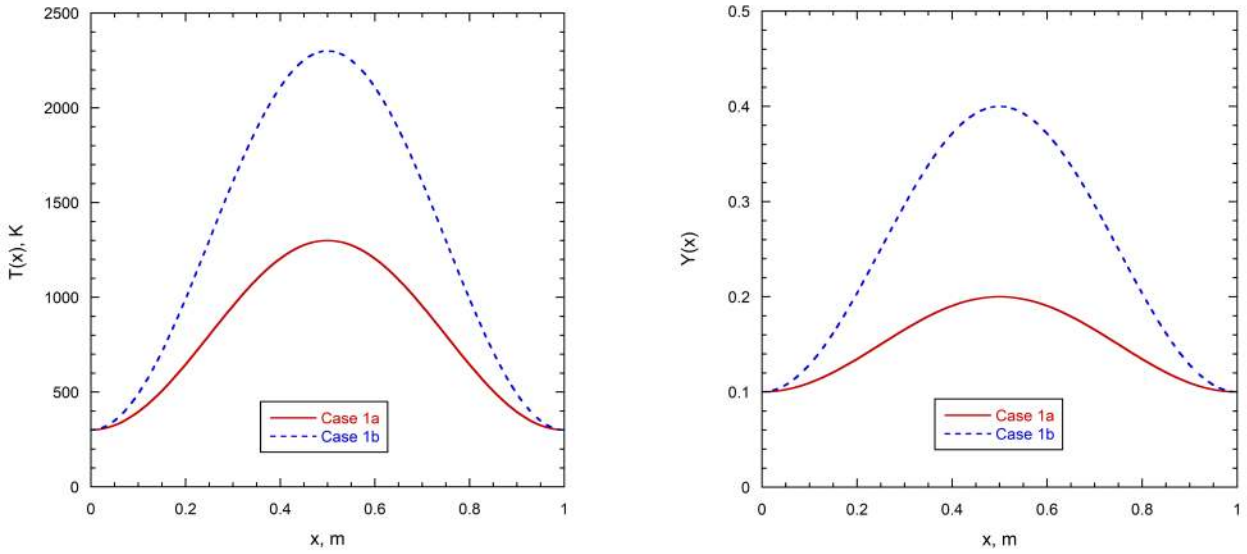

Figure 5. Temperature and water vapor mole fraction for Example 1, Cases 1a and 1b.

These two cases explore different temperature and mole fraction ranges, with corresponding significantly different temperature gradients and corresponding differences in absorption spectra. The analytical multilayer solution of the monochromatic RTE [19] was solved with the physical system discretized into 100 uniform spatial sublayers. Accuracy of the FSCK-I, FSCK-II, and RC-FSK models is evaluated in this example problem and Example 2 to follow by comparison with the rigorous line-by-line solutions using the absolute relative error $LE(x)$ defined as

$$LE(x) = \left|Q_{LBL}(x) - Q_{FSK}(x)\right| \Big/ \max\left|Q_{LBL}(x)\right| \times 100\% \tag{19}$$

and the total absolute relative error TE given by

$$TE = \int_0^L \left|Q_{LBL}(x) - Q_{FSK}(x)\right| dx \Bigg/ \int_0^L \left|Q_{LBL}(x)\right| dx \times 100\% \tag{20}$$

The absolute relative error in the prediction of the total net radiative flux at the wall is defined as

$$EF = \left|q_{LBL}(L) - q_{FSK}(L)\right| \Big/ \left|q_{LBL}(L)\right| \times 100\% \tag{21}$$

Figures 6a and 6b show predicted profiles of the total divergence of the net radiative flux for Cases 1a and 1b, respectively, using the FSCK-I, FSCK-II, and Rank Correlated FSK models,

along with the LBL benchmark solution. The reference temperature was set to the spatial average temperature $T_0 = T_{ave}$ for predictions using the FSCK-II model, and as the blackbody source temperature $T_P = T_{ave}$ for the RC-FSK method. For the FSCK-I model it will be shown for Examples 1 and 2 hereafter that the maximum temperature in the layer yields more accurate predictions, and was therefore used as the reference temperature, $T_0 = T_{\max}$.

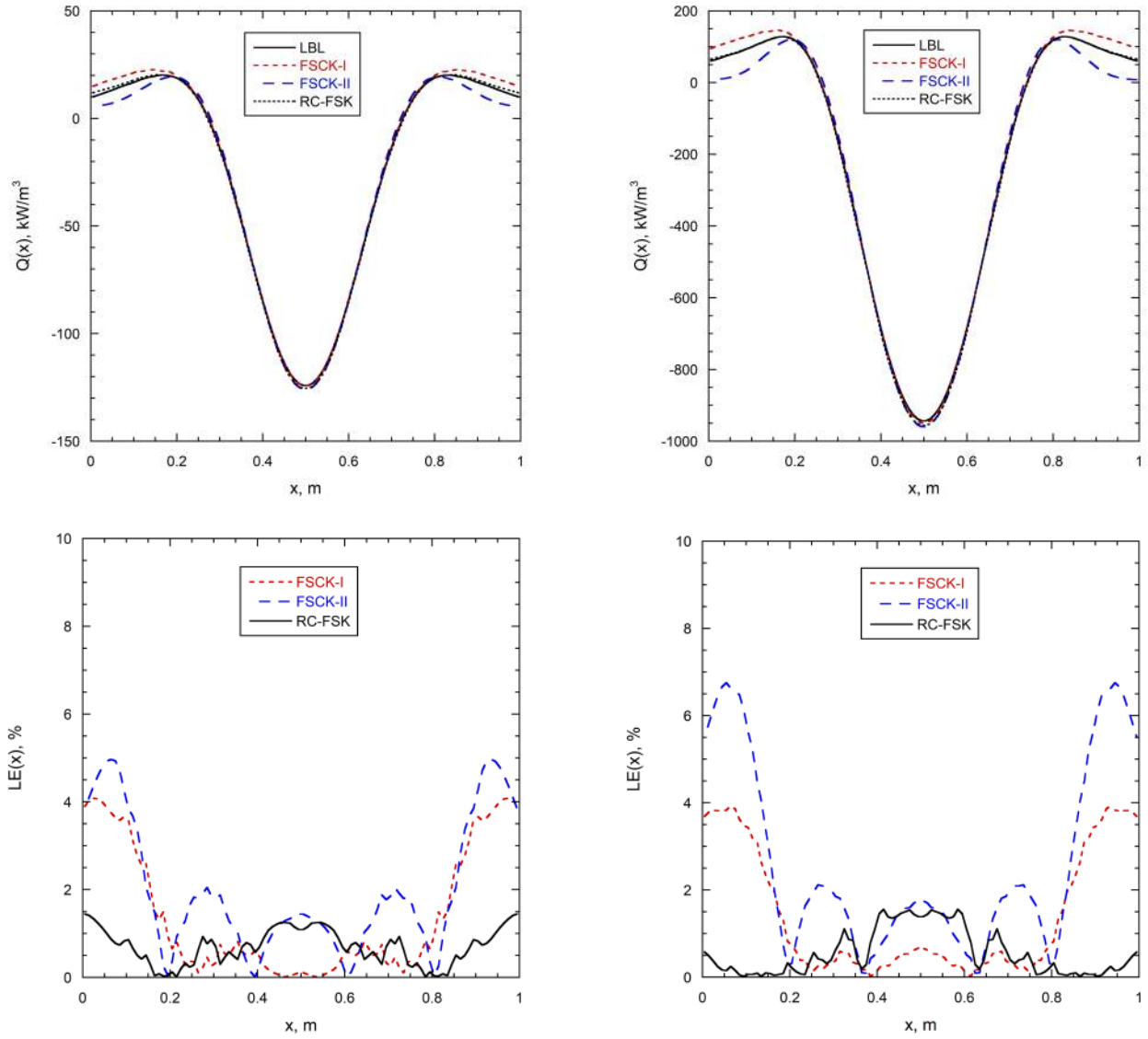

(a) (b)

Figure 6. Predicted local divergence of the net radiative flux, $Q(x)$, and local absolute relative error in the divergence prediction, $LE(x)$, for Example 1: a) Case 1a, and b) Case 1b.

Figure 6 reveals that all three FSK model formulations show good accuracy in the prediction of the local radiative flux divergence. Inaccuracies are confined principally to the coldest regions near the walls. Not surprisingly, the prediction error is somewhat higher for Case 1b, which features the radically higher temperature range.

The local absolute relative error shown in Fig. 6 for Example 1 shows that all three correlated FSK models yield good predictions, with the peak local error less than about 6%. For this scenario, the RC-FSK model appears to yield better accuracy than either the FSCK-I or FSCK-II models. Indeed, the maximum local error in the RC-FSK model predictions is less than 2%. Again it is noted that the local error is higher for the higher temperature case, but the increased error is rather modest for all three correlated FSK models.

Table 1 lists the total absolute relative error in local radiative flux divergence, *TE*, calculated according to Eq. (20) for the two cases of Example 1. Surprisingly, the FSCK-II (improved FSCK) model yields somewhat higher total error than the FSCK-I (original FSCK) model for this example problem. It should be mentioned that the FSCK-II model has been previously shown generally to yield improved predictive accuracy in other scenarios [18]. Table 1 shows that the total absolute relative error for the RC-FSK model is approximately 2% for both temperature/mole fraction ranges in Cases 1a and 1b, rather significantly lower than the previous correlated FSK formulations.

Table 1. Total relative error in the predicted radiative flux divergence for the FSCK-I, FSCK-II, and RC-FSK models for Example 1.

	Total Relative Error in Divergence, *TE*, %		
	FSCK-I	FSCK-II	RC-FSK
Case 1a	4.43%	6.22%	2.18%
Case 1b	4.33%	8.02%	1.70%

Table 2 shows the total wall radiant flux predicted using the line-by-line (LBL) solution and the three correlated FSK formulations for Cases 1a and 1b of Example 1. All three FSK formulations yield good results, but it appears that the RC-FSK prediction features somewhat

better accuracy than the FSCK-I and FSCK-II models. While this is not an exhaustive study, it does suggest that the Rank Correlated FSK implementation yields improvement in accuracy over previous correlated FSK approaches. This is consistent with the findings for the Rank Correlated SLW model, which was shown to yield improved predictive accuracy relative to the SLW Reference Approach [10].

Table 2. Predicted net radiant flux at the wall and absolute relative error in the wall flux, *EF*, for the FSCK-I, FSCK-II, and RC-FSK models for Example 1. The line-by-line benchmark prediction is also shown.

		Net radiant wall flux, kW/m^2 / Relative error in flux, *EF*, %		
	LBL, kW/m^2	FSCK-I	FSCK-II	RC-FSK
Case 1a	11.91	11.02 / 7.44%	12.55 / 5.41%	12.00 / 0.75%
Case 1b	106.49	100.62 / 5.50%	114.35 / 7.38%	108.60 / 1.99%

The sensitivity of model predictions to the gas reference temperature T_0 (or sensitivity to the blackbody source temperature T_P in the RC-FSK model) is shown in Fig. 7 for the FSCK-I, FSCK-II, and RC-FSK models using 25 quadrature points in the FSK solution of the RTE, Eq. (7). The figure illustrates the total absolute relative error in radiative flux divergence, *TE*, as a function of the value of T_0 (or T_P in the case of the RC-FSK model) specified in the simulation over the full range of temperature in the domain, $T_{\min} < T_0 < T_{\max}$ for both Case 1a and 1b in Example 1.

One may recall that the specification of the blackbody source temperature T_P should be a mathematical convenience [17]. However, Fig. 7 reveals that all models reveal some dependence on the specified blackbody temperature. The FSCK-I model exhibits the greatest sensitivity to blackbody source temperature, with total error decreasing from a maximum at $T_0 = T_P = T_{\min}$ to a minimum at $T_0 = T_P = T_{\max}$. However, the FSCK-I model has the advantage that the error decreases monotonically with increases in T_0, making it easier to specify the optimal reference temperature for this method. (It is for this reason that the maximum temperature in the domain was selected as reference temperature for the FSCK-I model predictions in the example problems investigated.) By contrast, the FSCK-II and RC-FSK models both exhibit significantly reduced

dependence on the reference temperature, and both show a local minimum in the total error behavior. The local minimum is near $T_0 = T_{ave}$ for the RC-FSK model, and at a somewhat lower reference temperature for the FSCK-II model. Of the three correlated FSK models, the FSCK-II model is seen to be the least sensitive to T_0 used in the simulation for this example problem.

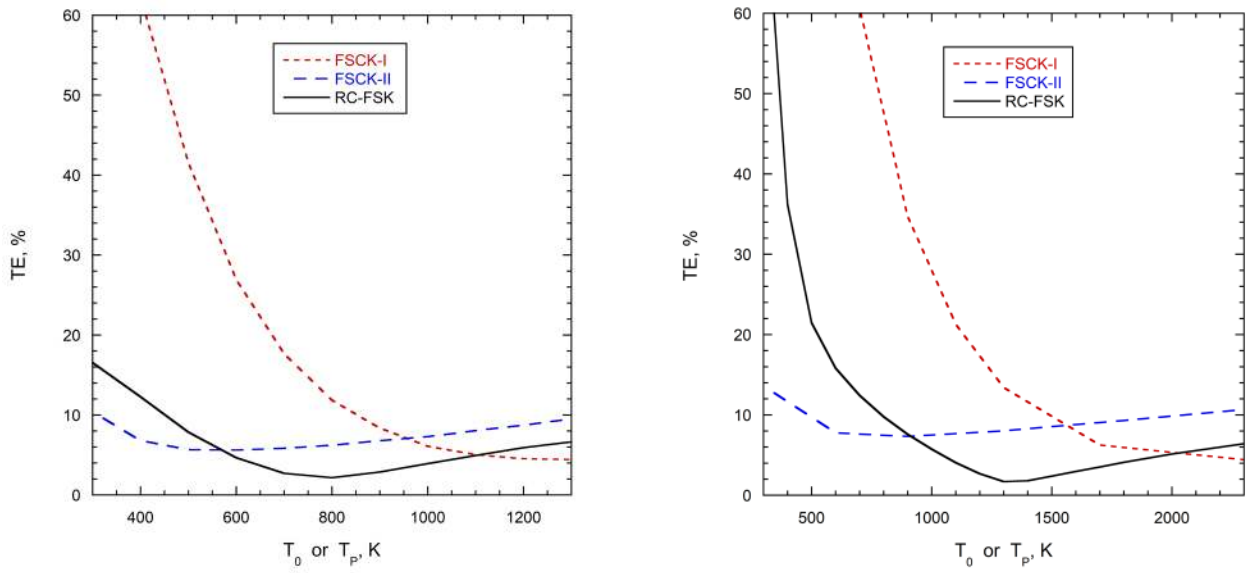

Figure 7. Sensitivity of predictions to the choice of reference temperature T_0 for the FSCK-I and FSCK-II models, and to the choice of T_P for the RC-FSK model for Example 1: a) Case 1a, and b) Case 1b.

Figure 8 illustrates the dependence of the total absolute relative error in the RC-FSK solution for Example 1, Case 1b on the number of quadrature points used in the solution of the RTE, Eq. (7). Figure 8a shows the variation of total error, *TE*, on the number of quadrature points in the RC-FSK solution for five different reference temperatures, T_P, ranging from $T_P = T_{\min}$ to $T_P = T_{\max}$. Note that while the dependence of total error on the number of quadrature points is quite minimal for $T_P > T_{ave}$, the error becomes increasingly dependent on the number of quadrature points as $T_P \to T_{\min}$. Indeed, it was found that for $T_P = T_{\min}$ more than 500 quadrature points are needed to accurately integrate the RTE. This is likely due to the need for greater resolution in the finite difference evaluation of the stretching function $a(g_0)$ in Eq. (10). It should be noted that

while 500 points may produce accurate solutions for the radiative transfer, this resolution is impractical in engineering computations.

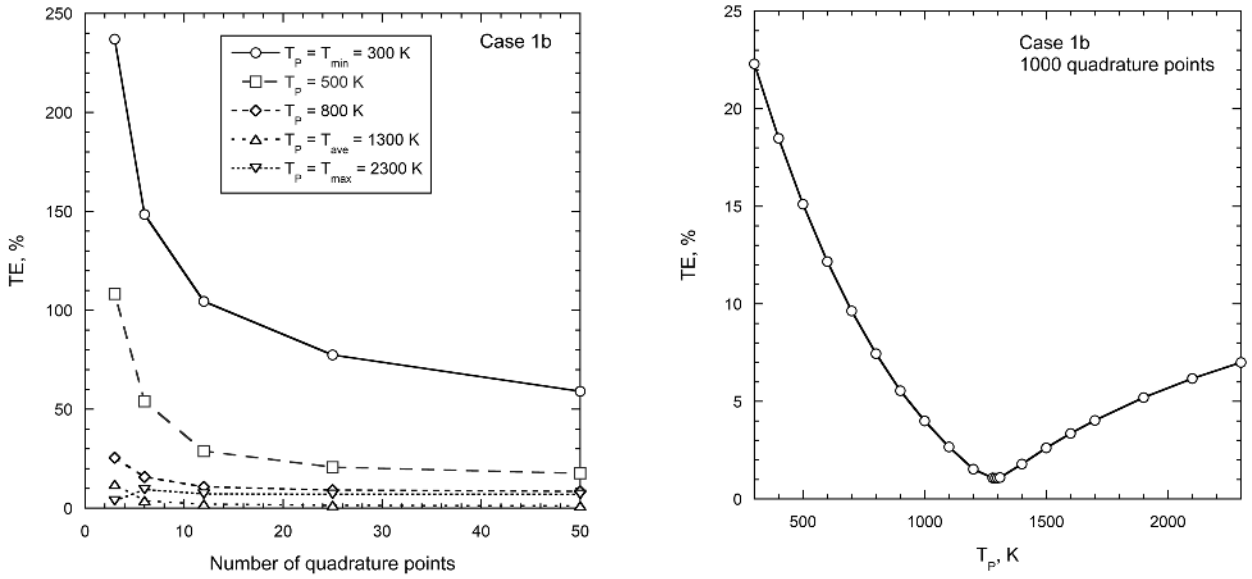

(a) (b)

Figure 8. Sensitivity of RC-FSK predictions for Example 1, Case 1b to a) the number of quadrature points employed in the RTE solution, and b) the reference blackbody source temperature T_P using 1000 quadrature points in the solution.

Figure 8b shows the variation of total error *TE* with reference temperature T_P for the RC-FSK prediction of Example 1, Case 1b employing 1000 quadrature points in the simulation. This extreme resolution in the solution of the RTE ensures that the dependence of the error is due only to the choice of reference temperature T_P, and not to the discretization error in the numerical evaluation of the stretching function, $a(g_0)$. Figure 8b reveals a local minimum in the total error for this case near $T_P = T_{ave}$, where *TE* is nominally 1%. One must hasten to mention that this observation may not be generalized based on this single example problem. However, for $T_P = T_{ave}$ this level of accuracy is quite extraordinary, given the extreme variation in temperature for Case 1b (T_{min} = 300 K, T_{max} = 2300 K) and the expected degree of corresponding uncorrelated behavior in the spectral absorption coefficient. The reason for the local minimum is not clear, given that it has been long acknowledged that the choice of blackbody source temperature T_P is a mathematical convenience. However, it suggests that there must be a theoretical foundation for

the existence of an optimal reference blackbody spectrum for this case, and that *k*-distributions can be constructed with arbitrary measures. However, the existence of an optimal measure may be possible, and it is observed in this work that the optimal measure is very likely close to the one based on the blackbody source at T_{ave}.

Example 2. Double wave profile of temperature and gas composition

Consider now the prediction of the local divergence of total net radiative flux in a plane-parallel layer of thickness L = 1.0 m bounded by black walls and filled with pure water vapor at total pressure p = 1.0 atm. As with Example 1, results are presented here for the predicted total net radiative wall flux and local divergence of the total net radiative flux in the layer. In this example double wave sinusoidal gas temperature and water vapor mole fraction profiles are imposed in the layer:

$$T(x)=\frac{T_{\max}+T_{\min}}{2}+\frac{T_{\max}-T_{\min}}{2}\cos\left[\frac{4\pi}{L}\left(x-\frac{L}{4}\right)\right], \text{ K} \tag{22a}$$

$$Y(x)=\frac{Y_{\max}+Y_{\min}}{2}+\frac{Y_{\max}-Y_{\min}}{2}\cos\left[\frac{4\pi}{L}\left(x-\frac{L}{4}\right)\right] \tag{22b}$$

as illustrated in Fig. 9. Wall temperatures are $T(0)=T(L)=T_{\min}$, K, and for this case $T_{\min}$ = 500 K, $T_{\max}$ = 1500 K (T_{ave} = 1000 K), and $Y_{\min}$ = 0.2, $Y_{\max}$ = 0.4 (Y_{ave} = 0.3).

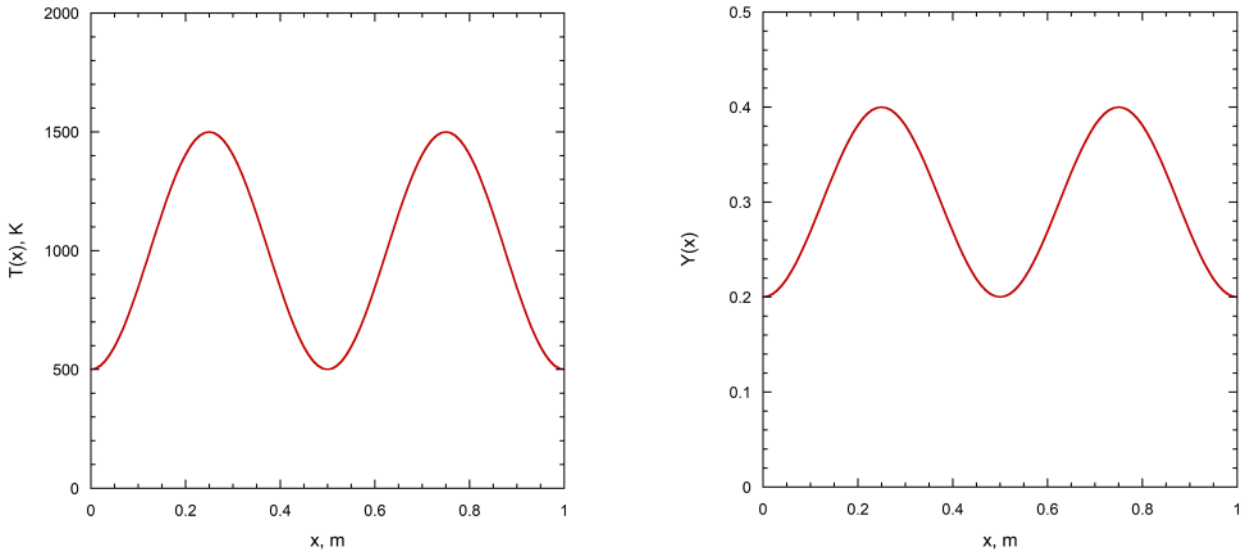

Figure 9. Temperature and water vapor mole fraction profiles for Example 2

As with Example 1, $T_0 = T_{\max}$ was used in the FSCK-I predictions, and $T_0 = T_{ave}$ and $T_P = T_{ave}$ were used, respectively, in the FSCK-II and RC-FSK simulations. This double wave profile is representative of what might be encountered in the developing region of a diffusion flame, and represents higher temperature gradients, a local minimum in temperature and concentration, and a generally more complex prediction challenge. Again, the analytical multilayer solution of the monochromatic RTE [19] was solved with the physical system discretized into 100 uniform spatial sublayers.

Figure 10 illustrates the predicted local radiative flux divergence $Q(x)$ and corresponding local error in flux divergence $LE(x)$ for the double wave temperature and gas concentration profiles of Example 2 for the three FSK model formulations. It should again be emphasized that the LBL benchmark prediction and all FSK model simulations were performed using the same spectral database [12]. As with the single wave problem of Example 1, the largest deviation in local radiative flux divergence from the line-by-line benchmark seen in Fig. 10 occurs in regions of low gas temperature. Nevertheless, the three FSK models yield very good accuracy. The local relative error, $LE(x)$, never exceeds 6% for any of the FSK model formulations. Further, it is difficult to draw definitive conclusions from this figure regarding relative accuracy among the three models.

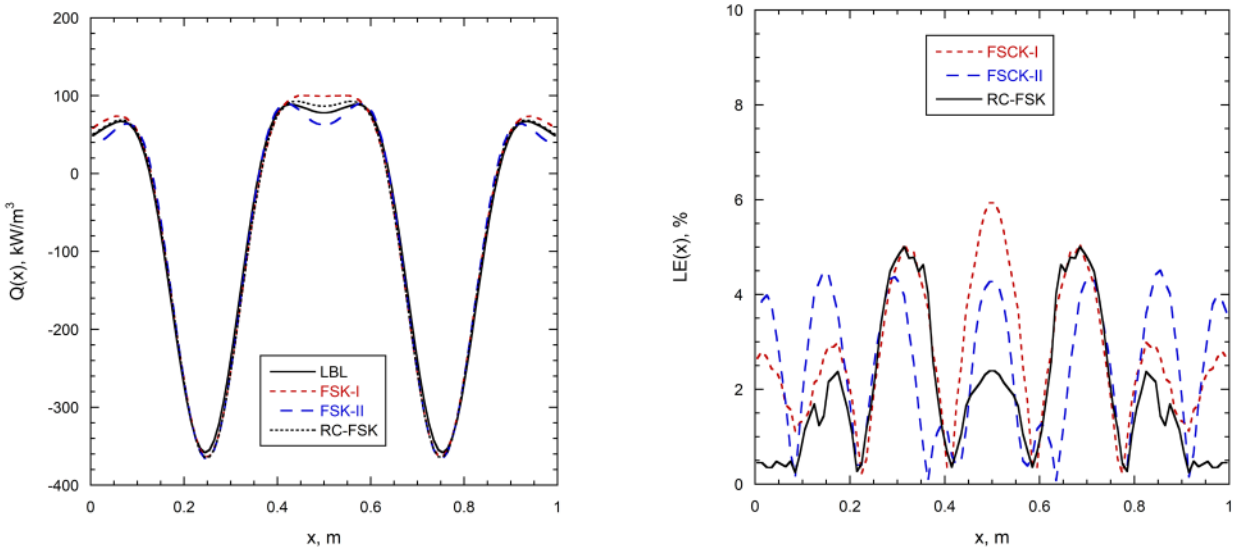

Figure 10. Predicted local divergence of the net radiative flux, $Q(x)$, and local absolute relative error in divergence prediction, $LE(x)$, for the double wave profiles of Example 2.

Table 3 lists the total relative error in the prediction of Example 2 for the FSCK-I, FSCK-II, and RC-FSK models. The total relative error is very close for all three correlated FSK models, with the RC-FSK model yielding modestly lower total error.

Table 3. Total relative error in the predicted radiative flux divergence for the FSCK-I, FSCK-II, and RC-FSK models for Example 2.

Total Relative Error in Flux Divergence, *TE*, %		
FSCK-I	FSCK-II	RC-FSK
7.62%	6.82%	5.37%

Table 4 shows the predicted net radiant flux at the wall using the three FSK models for Example 2. All three models yield good accuracy with the maximum relative error in wall flux found with the FSCK-II model at 4.33%. The error in wall flux prediction for both the FSCK-I and RC-FSK models is below 3%.

Table 4. Predicted net radiant flux at the wall and absolute relative error in the wall flux, *EF*, for the FSCK-I, FSCK-II, and RC-FSK models for Example 2. The line-by-line benchmark prediction is also shown.

	Net radiant wall flux, kW/m^2 / Relative error in flux, *EF*, %		
LBL, kW/m^2	FSCK-I	FSCK-II	RC-FSK
31.63	30.81 / 2.59%	33.00 / 4.33%	32.53 / 2.84%

Figure 11 illustrates the sensitivity of the accuracy in the prediction of the total relative error of radiative flux divergence to the choice of reference temperature T_0 for the FSCK-I and FSCK-II models, and T_P for the RC-FSK model for Example 2. Again, these data are for predictions made using 25 quadrature points in the solution of the RTE.

As was the case with the single wave profile of Example 1, Fig. 11 shows that the accuracy of the FSCK-I model exhibits the greatest sensitivity to T_0, and shows a monotonic decrease in the total error *TE* with increasing T_0. The FSCK-II and RC-FSK models exhibit considerably less

sensitivity to T_0 (or T_P in the case of the RC-FSK model), with the total error varying by only a few percent over the full range of reference temperature in the example. The total error for the RC-FSK model predictions is the lowest of all FSK models when T_P near the average temperature in the domain is selected.

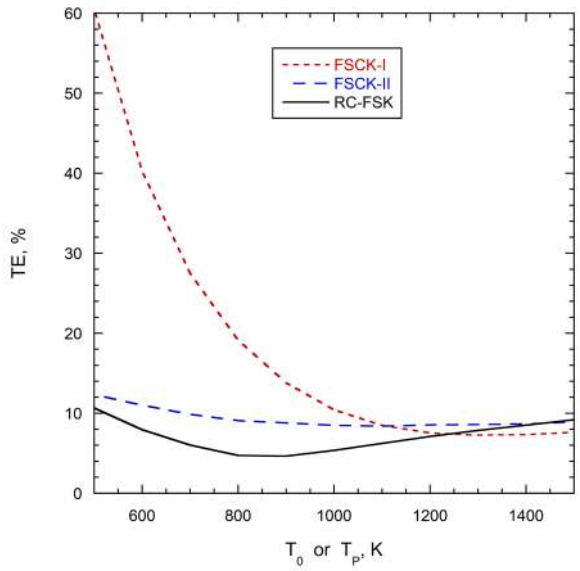

Figure 11. Sensitivity of predictions to the choice of reference temperature T_0 for the FSCK-I and FSCK-II models, and to the choice of T_P for the RC-FSK model for Example 2.

Example 3. Two-layer system

The final example is adapted from Pierrot *et al*. [4], and used by Cai and Modest [18] in the evaluation of FSCK models. A mixture of gases comprised of 10% CO_2, 20% H_2O, and 70% N_2 at a total pressure of 1 atm is confined in plane parallel domain bounded by cold, black walls. The gas mixture includes a hot isothermal layer of fixed width L_{hot} = 0.5 m at temperature T_{hot} = 2000 K, and a cold isothermal layer of variable length L_{cold} at temperature T_{cold} = 300 K. This problem explores an extreme case in which the absorption spectra at the two temperatures, T_{hot} = 2000 K and T_{cold} = 300 K, are almost statistically independent. The normalized directional total radiative flux leaving the cold layer at $L = L_{hot} + L_{cold}$ is predicted as a function of the cold layer thickness, L_{cold}, using the analytical solution for a two-layer system given in [19]. FSCK-I, FSCK-II, and RC-FSK solutions were generated using 25 quadrature points in the simulations, and the line-by-line benchmark solution was determined using the same parameters outlined for

the benchmark solutions in the previous example problems. Generally, all simulations in this example problem were carried out using $T_0 = T_{ave}$, with the exception of the FSCK-I model for which simulations using $T_0 = T_{\max}$ were also conducted to illustrate the sensitivity of exiting radiative flux to the reference temperature. It should be further noted here that, as defined in Eq. (16), the spatial average temperature T_{ave} for this two-layer problem is a function of L_{cold}. The reference temperature falls from T_{hot} as $L_{cold} \to 0$ toward T_{cold} as $L_{cold} \to \infty$.

Figure 12a shows the normalized total directional flux leaving the layer, $q(L)/E_b(T_{hot})$, as a function of the cold layer thickness, L_{cold}. Figure 12b illustrates the corresponding absolute error in the predicted normalized direction exit flux, defined as

$$ENF = \left| q_{LBL}(L) - q_{FSK}(L) \right| / q_{LBL}(L) \times 100\% \tag{23}$$

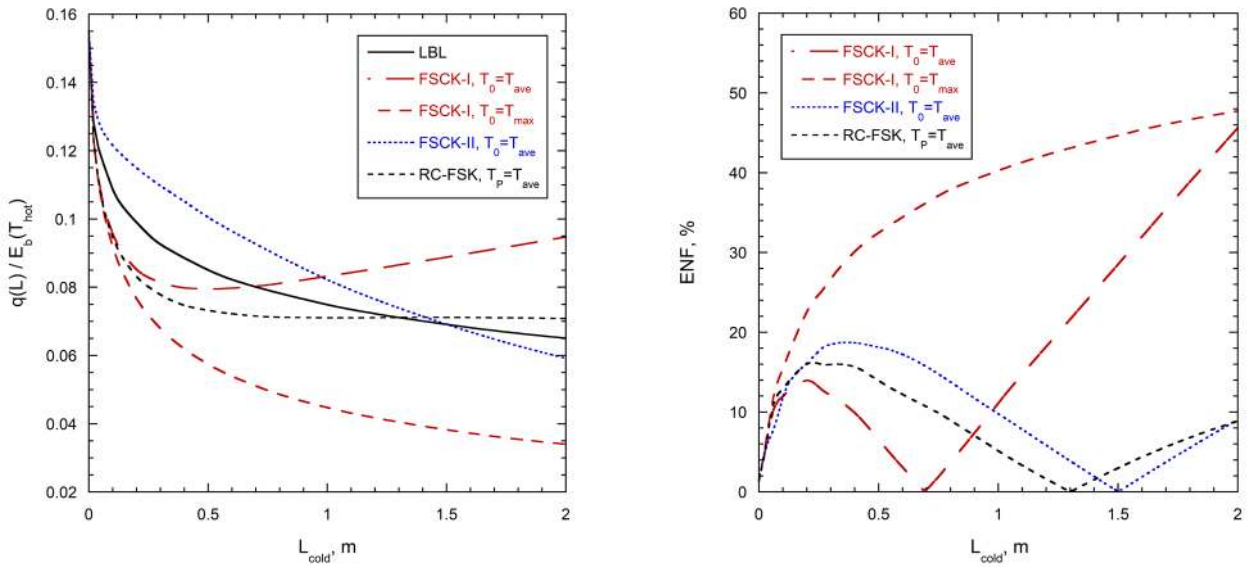

(a) (b)

Figure 12. Prediction of a) normalized total directional exit flux, $q(L)/E_b(T_P)$ and b) absolute error in predicted normalized exit flux, *ENF*, for the two-layer system of Example 3.

Figure 12 reveals that all FSK formulations approach the same predicted exit flux with good accuracy as the cold layer thickness vanishes. The models exhibit departure from the line-by-line benchmark as L_{cold} increases until the error reaches a maximum. With the exception of the FSCK-I model using $T_0 = T_{\max}$, the error then falls to zero, and rises (which is an artifact of the

error in normalized exit flux changing sign) as the cold layer thickness continues to increase. The FSCK-I model using $T_0 = T_{\max}$ yields the highest error at all values of L_{cold}. Although the FSCK-I model using $T_0 = T_{ave}$ shows moderately better accuracy than either the FSCK-II or RC-FSK models at small L_{cold}, the error for this model increases dramatically for $L_{cold} > 0.7$ m. The FSCK-II and RC-FSK models both exhibit much better accuracy than the FSCK-I model at large L_{cold}, at least for the range of L_{cold} investigated here.

It should be mentioned that all of the correlated FSK models explored here invoke the assumption of a correlated spectrum in some form to treat the spatial non-uniformities in the gas spectrum, and therefore, none is without error in their predictive accuracy. However, the development presented here suggests that the RC-FSK model is simpler in its construction and implementation, requires the specification of no reference state, requires only two cumulative distribution functions in implementing the correlated spectrum assumption, and example problems explored here suggest that the RC-FSK method may have some advantage with regard to accuracy relative to the FSCK-I and FSCK-II models. The FSCK-I and FSCK-II models have been widely adopted and confidently used in both research and engineering application settings. Reformulating a computational code based on either of these methods to incorporate the rank correlated spectrum assumption shown in the RC-FSK presented here would be a minor change.

4. CONCLUSIONS

Extending previous work on the Rank Correlated SLW (RC-SLW) model, the Rank Correlated FSK (RC-FSK) model has been proposed. It is shown that the method requires only two cumulative distribution functions in invoking the correlated spectrum assumption, and no specification of a reference thermodynamic state is needed. From this perspective the RC-FSK method appears to have some advantage over previous correlated FSK model formulations. Further, predictions for the RC-FSK method and prior FSCK methods reveal that the RC-FSK method may offer somewhat improved accuracy. Predictions for both the RC-FSK model and the Improved FSK (FSCK-II) model exhibit much less sensitivity to the reference temperature (blackbody source temperature in the RC-FSK method) chosen than the FSCK-I model. It is also observed that significantly more quadrature points are needed to accurately resolve the FSK

solution of the RTE for low reference temperatures (those below the spatial average temperature in the system approaching the minimum domain). Finally, this work demonstrates that the rank correlated spectrum implementation of the full spectrum *k*-distribution method, the RC-FSK model, is identical to the Rank Correlated SLW method.

Acknowledgement

This work was partially supported by Institut National des Sciences Appliquées de Lyon, France.

5. REFERENCES

1. Solovjov VP, Webb BW, Andre F. Radiative Properties of Gases, In: Kulacki F, editor. Handbook of Thermal Science and Engineering, New York, Springer, 2017, p. 1-74.
2. Denison MK, Webb BW. A spectral line based weighted-sum-of-gray-gases model for arbitrary RTE solvers. ASME J. Heat Transfer 1993; 115:1004-1012.
3. Denison MK, Webb BW. The spectral line based weighted-sum-of-gray-gases model in non-isothermal non-homogeneous media. ASME J. Heat Transfer 1995; 117:359-365.
4. Pierrot L, Rivière Ph, Soufiani A, Taine J. A fictitious-gas-based absorption distribution function global model for radiative transfer in hot gases. J. Quant. Spectr. Rad. Transfer 1999; 62:609-624.
5. Modest MF, and Zhang H. The Full Spectrum Correlated-*k* Distribution for Thermal Radiation from Molecular Gas-Particulate Mixtures. ASME J. Heat Transfer 2002; 124:30-38.
6. Maurente A, Bruno AB, França FHR, Howell JR. Non-dimensional wavenumber in full-spectrum *k*-distribution computations with or without a reference state. J. Quant. Spectr. Rad. Transfer 2017; 196:222-229.
7. Andre F, Vaillon R. The spectral-line moment-based (SLMB) modeling of the wide band and global blackbody-weighted transmission function and cumulative distribution function of the absorption coefficient in uniform media. J. Quant. Spectr. Rad. Transfer 2008; 109:2401-2416.

8. Solovjov VP, Andre F, Lemonnier D, Webb BW. The generalized SLW model. Eurotherm Conference 105: Computational Thermal Radiation in Participating Media V, Journal of Physics: Conference Series 2016; 012022, 676:1-36.
9. Chu H, Liu F, Consalvi J-L. Relationship between the spectral line based weighted-sum-of-gray-gases model and the full spectrum *k*-distribution model. J. Quant. Spectr. Radiat. Transfer 2014; 143:111-120.
10. Solovjov VP, Andre F, Lemonnier D, Webb BW. The rank correlated SLW model of gas radiation in non-uniform media. J. Quant, Spectr. Rad. Transfer 2017; 197:26-44.
11. Andre F, Solovjov VP, Lemonnier D, Webb BW. Co-monotonic global spectral models of gas radiation in non-uniform media based on arbitrary probability measures: Theoretical foundations. J. Appl. Math. Modeling 2017; 50:741-754.
12. Rothman LS, Gordon LE, Barber RJ, Dothe H, Gamache RR, Goldman A, Perevalov VI, Tashkun SA, Tennyson J. HITEMP, the high-temperature molecular spectroscopic database. J. Quant. Spectr. Rad. Transfer 2010; 111:2139-2150.
13. Wang CJ, Ge WJ, Modest MF, He BS. A full-spectrum *k*-distribution look-up table for radiative transfer in nonhomogeneous gaseous media. J. Quant. Spectr. Rad. Transfer 2016; 168:46-56.
14. Wang CJ, Modest MF, He BS. Full-spectrum *k*-distribution look-up table for non-homogeneous gas-soot mixtures. J. Quant. Spectr. Rad. Transfer 2016; 176:129-136.
15. Pearson JT, Webb BW, Solovjov, Ma J. Efficient representation of the absorption line blackbody distribution function for H_2O, CO_2, and CO at variable temperature, mole fraction, and total pressure. J. Quant, Spectr. Rad. Transfer 2014; 138:82-96.
16. Modest MF. Narrow-band and full-spectrum *k*-distributions for radiative heat transfer—correlated-*k* vs. scaling approximation. J. Quant. Spectr. Rad. Transfer 2003; 76:69-83.
17. Modest MF. Radiative Heat Transfer, 3rd ed. New York; Academic Press, 2013.
18. Cai J, Modest MF. Improved full-spectrum *k*-distribution implementation for inhomogeneous media using a narrow-band database. J. Quant. Spectr. Rad. Transfer 2014; 141:65-72.
19. Solovjov VP, Webb BW. Multilayer modeling of radiative transfer by SLW and CW methods in non-isothermal gaseous media. J. Quant, Spectr. Radiat. Transfer 2008; 109:245-257.

20. Andre F, Hou L, Roger M, Vaillon R. The multispectral gas radiation modeling: A new theoretical framework based on a multidimensional approach to the *k*-distribution method. J. Quant. Spectr. Rad. Transfer 2014; 147:178-195.